A microperfused incubator for tissue mimetic 3D cultures

Jelena Vukasinovic · D. Kacy Cullen ·
Michelle C. LaPlaca · Ari Glezer

Abstract High density, three-dimensional (3D) cultures present physical similarities to *in vivo* tissue and are invaluable tools for pre-clinical therapeutic discoveries and development of tissue engineered constructs. Unfortunately, the use of dense cultures is hindered by intra-culture transport limits allowing just a few layer thick cultures for reproducible studies. In order to overcome diffusion limits in intra-culture nutrient and gas availability, a simple scalable microfluidic perfusion platform was developed and validated. A novel perfusion approach maintained laminar flow of nutrients through the culture to meet metabolic need, while removing depleted medium and catabolites. Velocity distributions and 3D flow patterns were measured using microscopic particle image velocimetry. The effectiveness of forced convection laminar perfusion was confirmed by culturing 700 μm thick neural-astrocytic (1:1) constructs at cell density approaching that of the brain (50,000 cells/mm^3). At the optimized flow rate of the nutrient medium, the culture viability reached 90% through the full construct thickness at 2 days of perfusion while unperfused controls exhibited widespread cell death. The membrane aerated perfusion platform was integrated within a miniature, imaging accessible enclosure enabling temperature and gas control of the culture environment. Temperature measurements demonstrated fast feedback response to environmental changes resulting in the maintenance of the physiological temperature within 37±0.2°C. Reproducible culturing of tissue equivalents within dynamically controlled environments will provide higher fidelity to *in vivo* function in an *in vitro* accessible format for cell-based assays and regenerative medicine.

Keywords Incubator · Bioreactor · Perfusion · Convection · 3D culture · Neuron

1 Introduction

Culturing cells *in vitro* is one of the cornerstones of modern biology. Unfortunately, even for extensively studied tissues, many factors that induce or stabilize differentiated phenotypes are weakly understood and difficult to mirror *in vitro* (Bhatia et al. 1999). While certainly useful in many contexts, standard 2D culture models are poor mimics of tissues *in vivo*. Cells sense and respond to topology, dimensionality and rigidity of their environment that is inadequately approximated by the flat dish two-dimensions (Schindler et al. 2006). In 2D cultures, the concentrations of soluble growth factors and oxygen tensions are abnormally high, while 3D cues, cell-cell and cell-matrix interactions are ill-defined or absent (El-Ali et al. 2006). For example, integrin-mediated cell contact with extracellular matrix (ECM) proteins is restricted in 2D cultures, yet it affects cellular morphology, gene expression and many functions such as proliferation, differentiation, migration and apoptosis (Boudreau and Jones 1999; Chen et al. 1997; Lelievre et al. 1998; Thomas et al. 2002; Walpita and Hay 2002).

J. Vukasinovic (✉) · A. Glezer
Woodruff School of Mechanical Engineering,
Georgia Institute of Technology,
771 Ferst Drive,
Atlanta, GA 30332-0405, USA
e-mail: jelena.vukasinovic@me.gatech.edu

D. K. Cullen · M. C. LaPlaca
Coulter Department of Biomedical Engineering,
Georgia Institute of Technology,
313 Ferst Drive,
Atlanta, GA 30332-0535, USA

3D cultures are increasingly implemented in biotechnology and drug discovery since the cellular behavior is much closer to that found *in vivo* (Editorial 2003; Smalley et al. 2006). For example, in tumor studies cells can be influenced to switch between malignant and non-malignant states in 3D but not in 2D cultures (Kenny and Bissell 2003; Weaver et al. 1997); in breast cancer studies normal and malignant cells are indistinguishable in 2D cultures (Fournier and Martin 2006); the proliferation rates of primary and embryonic stem cells differ significantly in 3D and 2D cultures (Brannvall et al. 2007; Liu et al. 2006); and many of the 2D cell based assays, such as cell migration and invasion, are not representative of the *in vivo* activity (Smalley et al. 2006; Zaman et al. 2006). The principal benefits of 3D cultures are the reproducible generation of cell populations with *in vivo*-like qualities that more closely mimic *in vivo* morphology, growth rates, contact geometries, transport properties, and *in vivo* functions in an *in vitro* accessible format.

A realistic approach to increase the control over cell–cell, cell-matrix and cell-soluble-cues interactions typical of *in vivo* cell environments is to homogeneously combine multiple, tissue representative, cell types within a 3D extracellular matrix (ECM) at *in vivo* like densities and cell ratios (Boudreau and Jones 1999; Schindler et al. 2006). Unfortunately, the higher the density and the thicker the culture, the more challenging it becomes to maintain it. In the absence of functional vasculature the inner core suffers necrosis due to diffusion limited supply of nutrients and gas, and the removal of catabolic waste. Tissue-mimetic constructs invariably decay commensurate with the degree of cell death in thick slices of the explanted tissue they are approximating (Stoppini et al. 1991). While the vascularization of tissue engineered constructs appears promising (Caspi et al. 2007; Kirkpatrick et al. 2003; Levenberg et al. 2005; Rouwkema et al. 2008), it still remains a major area of research and one of the greatest challenges in tissue engineering.

To satisfy the metabolic and homeostatic requirements of engineered tissue equivalents, our approach focuses on providing an adequate and consistent intra-culture perfusion in a thermally regulated environment. This has been realized by forcing the laminar flow of nutrients through the mass of cells, mimicking circulation, at flow rates that were not deleterious to the cells. Our recent work (Cullen et al. 2007) showed that forced convection intra-culture perfusion enhanced the viability of thick, 3D neural constructs that were engineered using dissociated cerebral cortices and a bioactive scaffold. The motivation for this work is three-fold: (i) enhance the viability of even higher-density and thicker constructs, (ii) provide actively controlled, stable culturing conditions to reduce the experimental uncertainty linking culture environment and cell behavior, and, (iii) allow quantifiable analyses and microscopic monitoring in real time.

2 Materials and methods

2.1 Incubator design, packaging and interfacing

The incubator (patent pending) used in the present study is shown in Fig. 1. It comprises a heated enclosure (1a), perfusion chamber (1b), membrane aerator (1c), heating element (1d), thermocouple sensors (1e), and gas (1f) and fluidic connections (1g). The enclosure ($5.1 \times 2.5 \times 1.8$ cm) has a removable, optically transparent top that facilitates the inspection, imaging, integration and packaging. The membrane aerator (1c) encapsulates the device, equilibrates the medium within the perfusion chamber (1b) and functions as an aseptic moisture guard. It consists of an optically clear semi-permeable membrane sealed to a Teflon holder by a silicone O-ring (Potter and DeMarse 2001). The semi-permeable membrane is permeable to gases (N_2, O_2, H_2 and CO_2) and impermeable to water and water vapor. The fact that the perfusion chamber is heated and vented facilitates the removal of bubbles during filling.

Forced convection of the appropriate gas, such as 5% CO_2/ 95% air, over a thin flexible heater warms the incubator. Heat dissipation is regulated by a controller (connected to a DC switching relay and a DC power supply) that maintains the temperature of the injected nutrient medium at $37 \pm 0.2°C$. Gas inlet and outlet ports have built-in check valves to ensure unidirectional gas flow

Fig. 1 Incubator comprising: (**a**) heated enclosure, (**b**) perfusion chamber, (**c**) membrane aerator, (**d**) heating element, (**e**) thermocouple sensor, (**f**) gas and (**g**) fluidic connections

5 cm
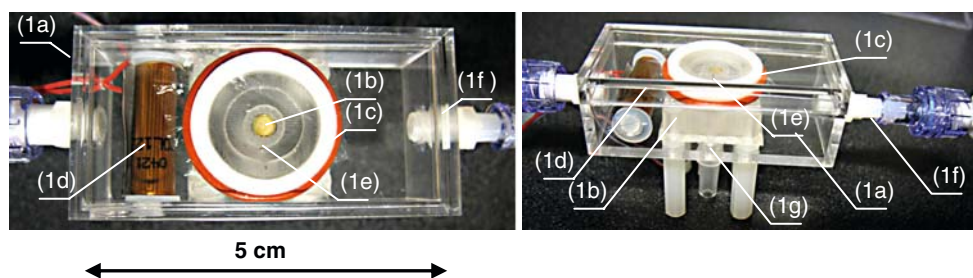
through the incubator. Luer-lock check valves are interfaced with rigid tubes connecting the incubator with another miniature enclosure termed the gas control enclosure. The gas control enclosure (Fig. 2) houses a pair of blowers and a shut-off valve connection to a gas bottle. The gas bottle contains a desired gas mixture, e.g. 5%CO_2/ 95% air and a miniature two-stage diaphragm pressure regulator (Beswick Engineering, Greenland, NH). The pressure regulator maintains a constant gas pressure within the gas control enclosure and the incubator. Two-stage design ensures downstream pressure regulated sustained low flow rate of gas through the regulator independent of the pressure of gas contained in the bottle. Miniature blowers (4 cm×4 cm× 4 cm, Thermaltake, City of Industry, CA) recirculate the gas through the incubator at a minimal noise level. Their speed and thus the gas flow rate are actively controlled using rheostats. Blowers, heater and temperature controller can each be battery operated to permit the portability of the system. The semi-permeable membrane aerator is also a moisture guard for the culture which eliminates the need for humidity control and sensing. Since unsaturated gas recirculates through the incubator the problems with condensation and unwanted growth of contaminating organisms are also eliminated.

2.2 Thermal design

Forced gas convection over a flexible heater (Minco, Minneapolis, MN) warms the gas injected into the incubator from the gas control enclosure. This creates a cylinder in a cross flow forced convection (Incropera and DeWitt 2002). The thermal design is sketched in Fig. 3. It is assumed that the heat dissipated by the heater Q_h pre-heats the gas from its inlet temperature $T_{a,i}$ to its heated
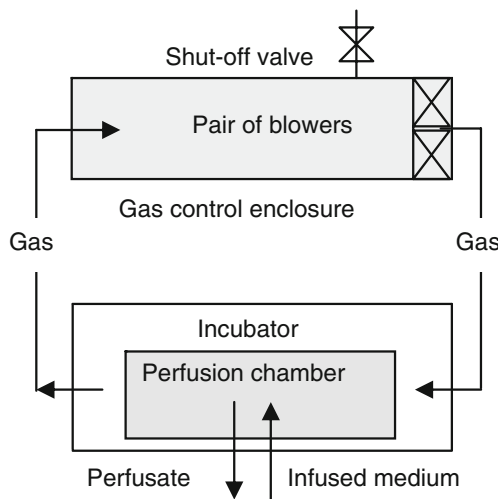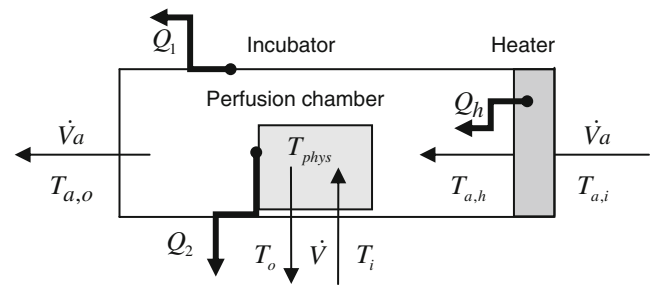

Fig. 3 Thermal design

temperature $T_{a,h}$. Pre-heated gas warms the interior of the incubator.

Typical heat losses are at the order of 1 W when the interior of the incubator is kept at a physiological temperature of T_{phys}=37°C and the ambient temperature is 20°C. The heat losses through the walls (Eq. 1) amount to Q_1=0.74 W (Incropera and DeWitt 2002) where A is the surface area of the incubator and ΔT=17°C the difference between the interior and exterior temperature. The overall heat transfer coefficient (Eq. 2) equals U=8.2 W/(m²·K) where t is the wall thickness and k is the thermal conductivity of the enclosure material and h=10 W/ (m²·K) is the coefficient of natural convection. To warm the nutrient medium from the ambient temperature to T_{phys} (Eq. 3) at the volume flow rate of $\dot{V}$=10 µL/min requires Q_2=0.012 W, where ρ, h_o and h_i are the density, the outlet and inlet enthalpy of the medium respectively. The medium properties are assumed to be equal to those of water.

Based on these losses, the needed gas volume flow rate through the incubator is $\dot{V}_a$=330 mL/s (Eq. 4) when the allowed temperature drop through the incubator (downstream from the heater) is ΔT_a=$T_{a,h}$ - $T_{a,o}$=2°C with ρ_a and c_p being the density and the specific heat capacity of air at 37°C (the averaged value of gas temperature through the incubator). For this calculation it is assumed that the gas is air, that the gas temperature immediately downstream of the heater is $T_{a,h}$=38°C and that the gas exit temperature is $T_{a,o}$=36°C. The estimated flow rate and the corresponding pressure drop through the incubator, the gas control enclosure, and the gas tubes were used to select the miniature blowers.

As forced convection of heated gas maintains desired temperatures, the heater needs to dissipate Q_h=7 W (Eq. 5) to pre-heat the gas from 20°C to 38°C (air properties are evaluated at the average temperature of 29°C). This power requirement was used to select the appropriate heater and power supply. In practice the heater dissipated just a few Watts mainly due to lower than assumed Q_1 losses (unheated gas entry length through the incubator) and partly due to higher temperature of the recirculated gas versus that of the ambient temperature.

Fig. 2 The gas control enclosure

Another important parameter in designing the incubator is the heated tube entry length required to pre-heat the medium to T_{phys} before entering the culture chamber. The length of infusion tube within the incubator needs to be at least $L=$ 550 µm (Eq. 6) to satisfy this demand at $\dot{V}=10$ µL/min with the internal tube diameter of $D=2$ mm (Incropera and DeWitt 2002). Assuming that the exterior surface of the tube is isothermal at $T_s=38°C$ and that the inlet and outlet medium temperatures are $T_i=20°C$ and $T_o=37°C$, respectively, the logarithmic mean temperature difference is $\Delta T_{lm}=$ 5.9°C (Eq. 7), where $\Delta T_o=T_s - T_o$ and $\Delta T_i=T_s - T_i$. The averaged heat transfer coefficient (Eq. 8) is $h=949$ W/(m²·K), where $Nu=3.66$ is the Nusselt number for fully developed laminar flow in a circular tube of a uniform exterior temperature, and k is the thermal conductivity of water at the mean fluid temperature. When calculating h the flow was assumed to be hydrodynamically and thermally fully developed since the combined entry length is $l=57$ µm (Eq. 9), where Re_D and Pr are the Reynolds and the Prandtl numbers respectively, evaluated at the mean fluid temperature.

2.3 Microfluidic perfusion chamber design and fabrication

A microperfusion chamber (patent pending) with membrane aerator is shown in Fig. 4(a). It contains an inner culture chamber, an outer withdrawal chamber, an inlet and an outlet port [Fig. 4(b)]. Medium is infused into the culture chamber [Fig. 4(c)] via the inlet port and dispersed throughout the culture through the porous perfusion substrate that supports the culture. Culture is adhered to the interior of the culture chamber by adhesion-promoting ECM constituents. Depleted medium and catabolites are withdrawn from the culture through peripheral microchannels. The schematic of induced flow is shown in Fig. 4(d).
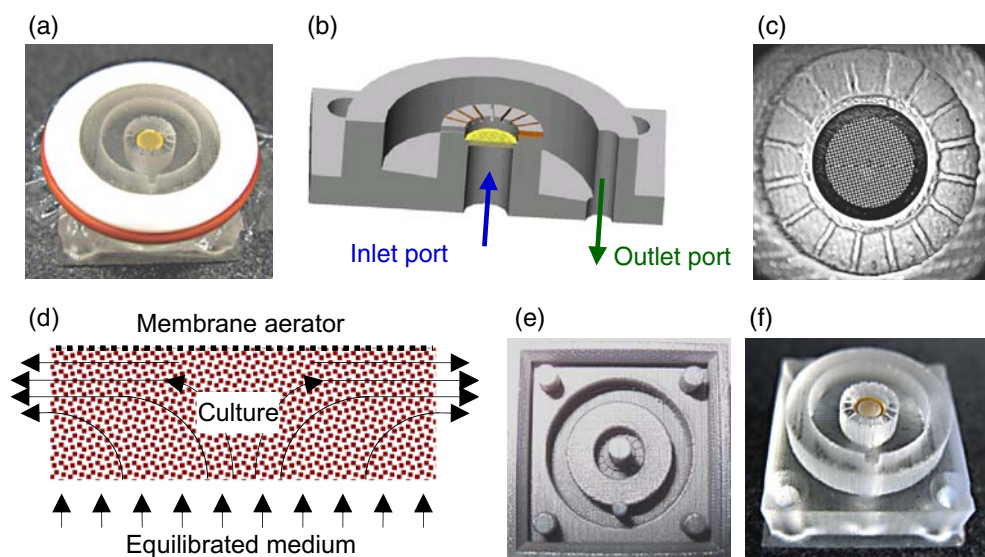
The perfusion substrate has 40% open area for fluid flow by 54 µm×54 µm openings. The culture chamber measures 3.5 mm in diameter and 700 µm in height [Fig. 4(c)]. The culture and withdrawal chamber are connected by 150 µm wide microchannels [Fig. 4(b),(c)] that start mid-height through the culture chamber and extend to its top. A membrane aerator, press-fit onto the top of the perfusion chamber, forces the radial outflow of perfusate through the microchannels, withdrawal chamber and outlet port. A syringe pump (KD Scientific, Holliston, MA) carrying opposing (infusion and withdrawal) syringes on a single drive, enables simultaneous medium infusion into the culture chamber and mass-equilibrated withdrawal of depleted medium and catabolites from the withdrawal chamber.

Biocompatible perfusion chambers were rapidly prototyped using solid object printing and soft lithography. Disposable, 3D molds [Fig. 4(e)] were extruded in a wax-based material using a 3D printer (Thermojet, 3D Systems, Rock Hill, SC). Feature resolution was ≤ 85 µm which is sufficient for our applications. Perfusion chambers were replica molded in polydimethylsiloxane (PDMS) using a 10:1 ratio of pre-polymer base and cross-linking agent (SYLGARD 184; Dow Corning, Midland, MI). A transmission electron microscopy grid (Ted Pella, Redding, CA) served as the perfusion substrate and was sealed to the bottom of the culture chamber by a thin layer of watertight PDMS [Fig. 4(f)]. Lastly, the assembled membrane aerator was press-fitted onto the perfusion chamber [Fig. 4(a)].

2.4 Flow and thermal diagnostics

Microscopic particle image velocimetry (Santiago et al. 1998) was used to characterize the flow within the culture chamber absent the culture. Fluid velocity was measured by

Fig. 4 Perfusion platform design and fabrication. (**a**) Perfusion platform comprising perfusion chamber and membrane aerator, (**b**) a cross section view of the perfusion chamber, (**c**) culture chamber, (**d**) schematic of the induced flow within the culture chamber, (**e**) wax mold and (**f**) PDMS replica with attached perfusion source

imaging the displacement of 550 nm fluorescent tracers suspended in DI water using an episcopic, darkfield fluorescence arrangement (Choi et al. 2008; Cullen et al. 2007). Particles were sufficiently small to faithfully follow the flow without influencing it [particle Stokes number ≪ 0.14; (Dring 1982)]. Velocity distributions were measured in planes that were parallel to the perfusion source by adjusting the distance between the perfusion chamber and the imaging optics. Sophisticated image processing and cross-correlation of particle images (Choi et al. 2008; Cullen et al. 2007) were used to extract velocity measurements at a resolution that was within 5% of the microjet injection velocity.

A closed-loop control system regulated the thermal environment. This system employed a proportional-integral-differential (PID series 96) controller (Watlow, St. Louis, MO) to regulate the voltage supplied to the heater based on the temperature measured just below the perfusion substrate by a thermocouple routed through a miniature nylon tee to minimally affect the flow. Temperature sensors were PFA Teflon insulated 127 µm T-type thermocouple probes (Omega Engineering, Stamford, CT). Conductive heat losses from the thermocouple junctions along the insulated lead wires were negligible (<0.1%). A Hydra 2620A portable data acquisition unit (Fluke Corporation, Everett, WA) interfaced to a host computer was used to sample the temperature at the rate of 10 Hz. The measurement resolution was 0.1°C.

2.5 3D co-culture perfusion experiments and viability assay

Prior to the start of perfusion all tubes were filled with the medium to eliminate bubbles. The medium was Neurobasal supplemented with 2% B-27, 1% G-5, 500µM L-glutamine, and 1% antibiotic/antimycotic. All culture reagents were from Invitrogen (Carlsbad, CA) or Sigma (St. Louis, MO) unless noted otherwise.

Standard isolation and culture techniques were used according to previous published procedures (Cullen et al. 2007). Primary E-18 cortical neurons and P1 astrocytes (1:1 ratio) were uniformly distributed within Matrigel® matrix (BD Biosciences, Bedford, MA), delivered into the culture chamber in a fluid-like state, and placed at 37°C and 5% CO_2-95% air for 45 min to gel. The plating density was 50,000 cells/mm^3 at 700µm thickness (prior to gelling) and the final protein concentration was 7.5 mg/mL. This provided adequate cellular adhesion to the interior of the culture chamber as verified by visual inspection and the scrapping of cultures at the end of perfusion experiments. After gelling, the perfusion chamber was fully submerged and perfusion initiated. Perfused co-cultures were subject to continuous infusion/withdrawal at rates of 0.5, 2 and 3 µL/min (i.e. 4, 16 and 24 culture volume exchanges/hour).

Unperfused controls had the medium changed daily ($n=4$). After 2 days *in vitro* (DIV), co-cultures ($n=4$–6 per condition) were labeled using a LIVE/DEAD Viability/Cytotoxicity Kit (Invitrogen) and imaged using confocal microscopy (Cullen et al. 2007). Multiple Z-stacks were captured across the thickness of co-cultures. Live and dead cells were counted manually from 20µm thick reconstructions as a function of distance from the perfusion source. General linear model ANOVA was used for statistical analysis followed by post-hoc Tukey's pair-wise comparisons ($p < 0.05$ was required for significance in either test). Data are presented as mean ± standard deviation.

3 Results

3.1 Fluidic validation

Schematic of the global, induced flow within continuously perfused culture chamber is shown in Fig. 4(d). Flow is engendered by an array of about 584 discrete microjets emanating from the porous grid and by radial withdrawal of perfusate through an array of 16 peripheral microchannels.

Measurement domain covers the center of the culture chamber with an array of approximately 5×5 openings in focus [Fig. 5(a)]. Velocity distributions were measured in planes that were parallel to the porous grid and normal to the axes of discharged microjets [Fig. 5(b–f)]. The elevation Z was measured from the perfusion source. The nominal volume flow rate through the perfusion chamber was 5µL/min (40 exchanges/hour) with microjet ejection velocity of 50µm/s. Flow near the perfusion source was characterized by the radial spreading of semi-confined, submerged, laminar microjets normal to their axes [Fig. 5(b)]. With increasing distance from the perfusion substrate, microjets accelerated radially [Fig. 5(c)] due to momentum exchange between the jets and the low momentum medium within the chamber. As a consequence of these shear driven interactions, jets broadened with concomitant reduction in their streamwise velocity (along their axes). A continuing momentum exchange and decrease in jet streamwise momentum caused the turning of discrete microjets from their nominally vertical trajectories and neighboring jets began to interfere. These interactions were accompanied by loss of coherence and merging of jet flows [Fig. 5(d),(e)]. Beyond mid-height through the chamber, peripheral fluid withdrawal directed the merging jet flows towards the exit microchannels [Fig. 5(f)].

3.2 3D co-culture perfusion

Forced convection interstitial perfusion was proven useful in overcoming diffusive limitations in 3D culture density
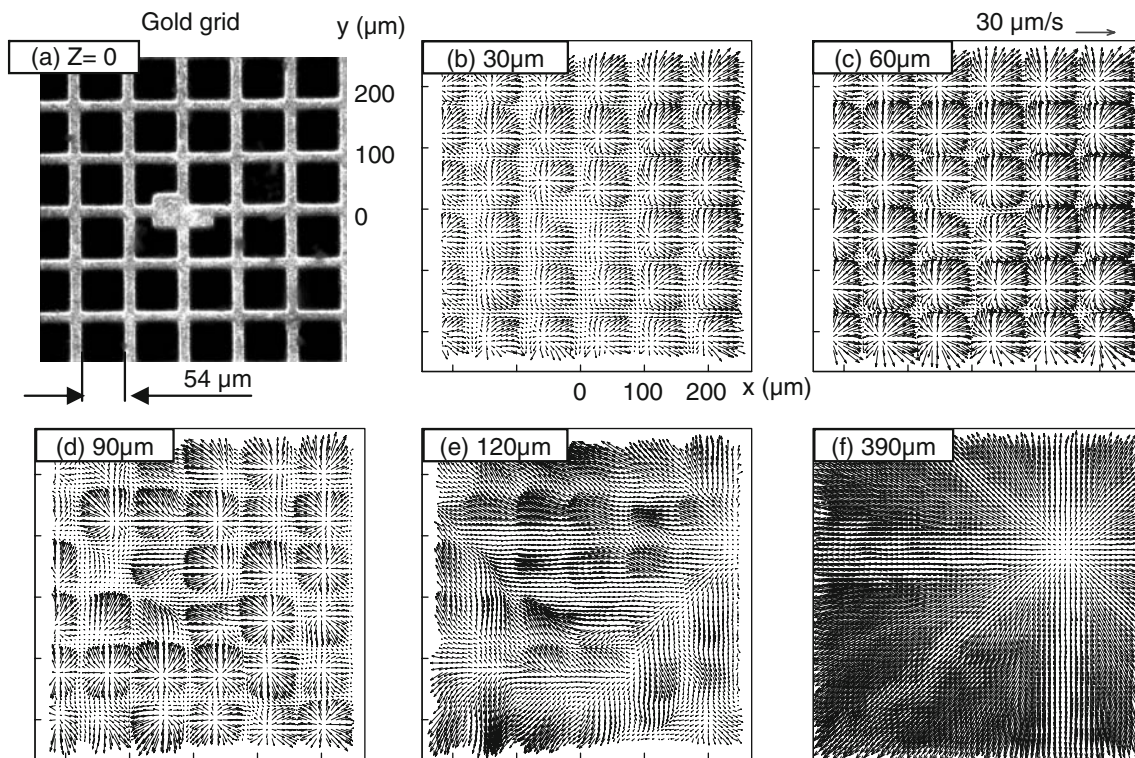
Fig. 5 MicroPIV measurements of the induced flow in the culture chamber as a function of distance (Z) from the perfusion source in planes normal to the axes of emanating microjets. (**a**) Filed of view.

(**b**) The radial spreading of discrete, submerged, laminar microjets upon injection. (**c**) The broadening of microjets. (**d**–**e**) Jet interactions and the loss of coherence. (**f**) Peripheral withdrawal of perfusate

and thickness [Fig. 6(a–e)]. At a plating density of 50,000 cells/mm^3 and nominally 700 μm pre-gelling thickness, unperfused but otherwise identical co-culture controls deteriorated and thinned down rapidly to a thickness of approximately 60 μm by 2 days post-plating [Fig. 6(a)]. Live cells fluoresce green (calcein+; via AM-cleavage),

while dead or dying cells have red fluorescing nuclei (EthD-1 binding to DNA). Although the remaining cells and the matrix adhered to the bottom of the culture chamber, the viability was poor and the density of remaining cells was low (<10% of that at plating). Perfused constructs had a higher cell density and viability that

Fig. 6 Live/dead 60 μm thick confocal micrographs from neural-astrocytic (1:1) constructs plated at 50,000 cells/mm^3 and 700 μm thickness. (**a**) Unperfused control culture imaged close to perfusion source and the middle of perfused constructs at (**b**) 0.5 μL/min, (**c**) 2 μL/min and (**d**) 3 μL/min. (**e**) 2 DIV viability through the construct thickness (culture bottom is the closest to perfusion source)
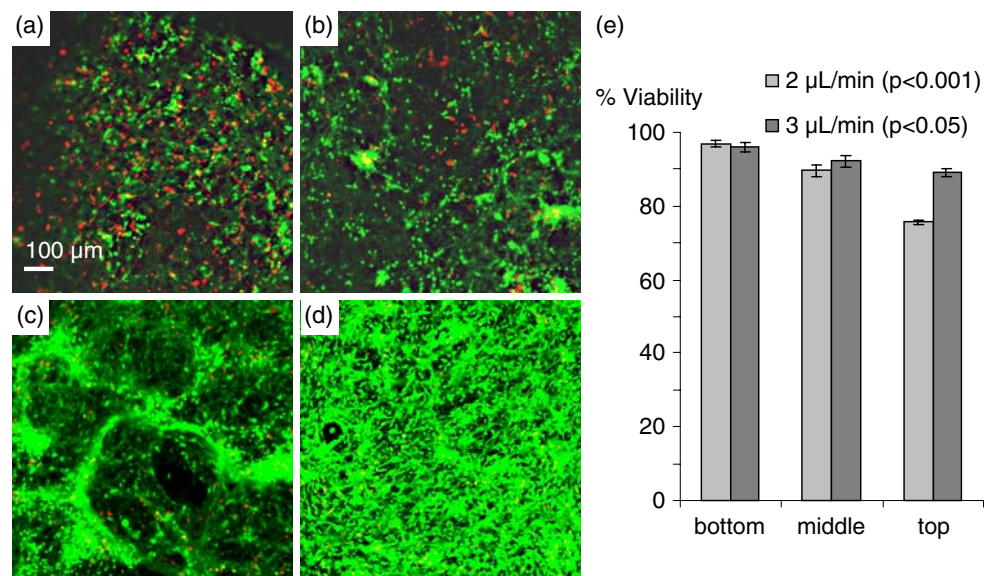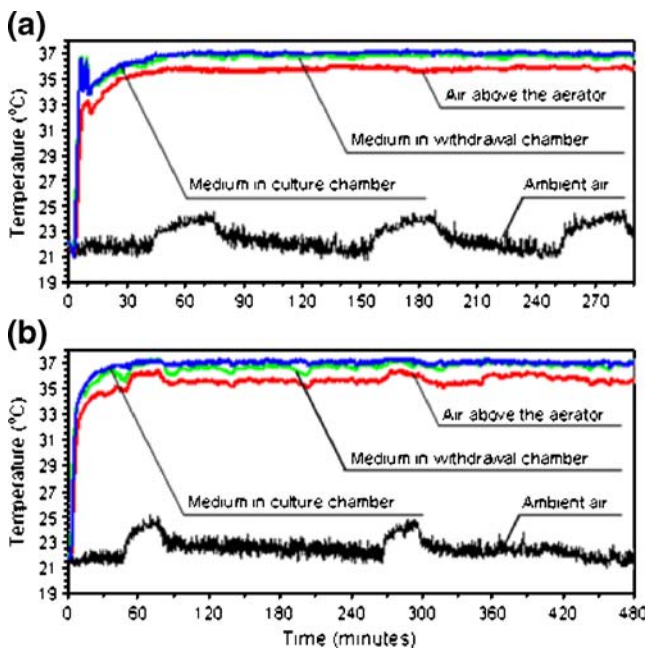
Fig. 7 Temperature measurements. (**a**) During a 4-hour period following device initiation and controller tuning. (**b**) During 8 h of operation after device initiation from the laboratory condition

monotonically increased with the increase in applied flow rates from 0.5 to 3 μL/min [Fig. 6(b–d)]. While low perfusion rates mitigate co-culture decay and thinning, an optimal exchange rate is required where cellular metabolic demands are equally satisfied through the full thickness of the co-culture without flow-induced cell damage. At flow rates that were lower than optimal, we expected our particular flow configuration to favor the bottom of the culture chamber (highest nutrient concentration). We found that the co-culture viability was statistically dependent on the proximity to perfusion source at both 2 μL/min ($p < 0.001$) and 3 μL/min ($p < 0.05$) [Fig. 6(e)]. At the rate of 3 μL/min (24 volume exchanges/hour), the live cell count was also statistically dependent on the elevation ($p < 0.001$). In the vicinity of the perfusion source there were $55,010 \pm 6,120$ live cells, $43,060 \pm 2,550$ in the middle portion of the construct, and $22,600 \pm 7,370$ cells at the top of the constructs (which were no less than 450–500 μm thick at 2 DIV).

3.3 Thermal validation

Temperature measurements are shown in Fig. 7(a),(b). The temperature of medium in the culture chamber corresponds to the thermocouple measurements taken just below the perfusion source. The temperature of medium in the withdrawal chamber was acquired by a thermocouple positioned about mid-height through the chamber and routed through the outlet port. The temperature of air

above the aerator was measured about mid-way between the aerator and the incubator cover top.

When the system is used for the first time in a given environment, the controller is auto-tuned to optimize the parameters for the PID closed-loop temperature control [Fig. 7 (a)]. This is executed only once provided that the environmental conditions during auto-tune are representative of the thermal environment in which the system is used. In laboratory conditions, the auto-tune lasted less than 15 min. The temperature of injected medium reached $T_{phys} = 37°C$ within 30 min following the controller tuning and remained steady thereafter. The nominal volume flow rate through the perfusion chamber was 10 μL/min (80 exchanges/hour).

Figure 7(b) shows 8-hour long temperature measurements after starting the device using the same set of control parameters acquired during tuning. Owing to a small thermal mass (compared to refrigerator-size incubators) and convective heat transport, the medium within the culture chamber rapidly attained T_{phys}. Consuming no more than a few Watts of power, desired temperature was reached within 45 min after starting the device, while it may take hours for large incubators to obtain the same after power loss. The temperature of injected medium remained steady to within $37 \pm 0.2°C$ thereafter.

The temperature of medium in the withdrawal chamber followed that of the injected medium. The absolute difference in these temperatures was, on the average, within 0.3°C. The thermocouple in withdrawal chamber was positioned 6.2 mm downstream of the center of the culture chamber in the direction of the forced air flow. Since this distance is approximately twice the culture chamber radius, it was assumed that the fluid temperature inside the culture chamber (located above the perfusion source and co-axially within the withdrawal chamber) remained spatially fairly uniform.

4 Discussion

Compared to cells grown in monolayers, 3D cultures are biochemically and physiologically more similar to *in vivo* tissues, yet technically quite challenging to maintain. Metabolic and homeostatic requirements of such cultures demand tight control of the cellular microenvironment, which can be sophisticated even in an attempt to maintain simplicity. The present study confirmed the following: (a) forced convection intra-culture perfusion supports dense, thick 3D cultures and (b) the environmental control of cellular microenvironment can be realized using forced convection of the nutrient medium and the heated gas while simultaneously allowing real-time culture imaging.

To the best of our knowledge, none of the perfusion systems (e.g. Zbicz- or Haas-top chambers for acute brain

slices; Harvard Apparatus, Holliston, MA) or bioreactors (Wang et al. 2005) employ the concept of forced interstitial nutrient circulation. Rather, medium is efficiently perfused around the tissue or engineered construct but not forced through the cultures. Due to lower resistance to fluid flow around the tissue than interstitially, the dominant mode of interstitial transport is molecular diffusion. The concentration of nutrients and dissolved gas, while high in the medium surrounding the tissue, reduces towards the tissue interior. Tissue fails to uniformly equilibrate with the extracellular environment, develops a necrotic core and deteriorates rapidly. This is more pronounced for dense and thick 3D cultures where diffusion limited mass transport is exacerbated.

4.1 Forced convection of the medium

Measured velocity distributions within the culture chamber confirm its fluidic functionality and reveal that the induced flow is three-dimensional even without the culture. Jet interactions (closer to perfusion source) were replaced by convectively biased flow towards peripheral exits (starting mid-height through the chamber). Convective circulation through the chamber, inducing large and small-scale motions, serves to enhance the mass transport beyond that of molecular diffusion. On a global scale, the steady exchange of momentum between infused and withdrawn medium is expected to facilitate the transport of small, as well as large molecules (e.g. proteins or growth factors having low diffusivities). Locally, small-scale jet interactions and fluid shear serve to improve the uniformity of the intra-culture nutrient availability.

4.2 3D culturing

The utility of perfusion was validated by culturing of primary 3D neuronal-astrocytic (1:1 ratio) constructs at a plating density that is approximately half the density found in many cortical regions (Bass et al. 1971; Braitenberg 2001; Gabbott and Stewart 1987; Sultan and Braitenberg 1993; Williams and Herrup 1988). We found that the increase in flow rates resulted in the improvement in culture viability. At flow rates that were insufficient to meet the cellular requirements throughout the full construct thickness, the viability was higher near the perfusion source and reduced towards the top of the culture. At the highest applied flow rate of 3 μL/min the culture viability, while reaching 90% through the full culture thickness, was still dependent on the proximity to the perfusion source, suggesting that a slightly higher flow rate may be required to abolish this dependency.

Lower cell densities from the culture bottom to the top can only be partly ascribed to the success of perfusion.

Specifically, a degree of cell settling within the matrix influences the cell density from the top to the bottom of the culture. During gelling some matrix and cell loss appear through the porous perfusion source (at the bottom of the culture chamber) therefore affecting the final construct thickness. However, even with these noted caveats, a forced interstitial convection at a rate of 3 μL/min reproducibly maintained ~90% cell viability across the thickness of the constructs that were no less than 450–500 μm thick at 2 DIV. Compared to our previous work (Cullen et al. 2007), the cell density was increased five-fold, cultures scaled-down, perfusion chamber miniaturized and integrated into a microscope accessible, centimeter-scale incubator providing stable culturing conditions during studies.

The upper limit on 3D culture thickness that can be reproducibly maintained *in vitro* using forced convection intra-culture perfusion was not investigated. For a given plating density and cell ratios, the maximum culture thickness is thought to depend on the structural strength, homogeneity and temporal stability of the ECM to support the cells in 3D; intra-culture reduction in nutrient and gas availability due to cellular consumption; the metabolic coupling between different cell types, such as neurometabolic coupling of synaptic activity and glucose utilization between neurons and glia (Deitmer 2001; Magistretti 2006; Tsacopoulos and Magistretti 1996); the accumulation of catabolites; concentration of cell secreted soluble cues, cell-cell and cell-matrix signaling; and flow-induced normal and shear stresses among other parameters. Nonetheless, even these limits may be exceeded by modifying the flow geometry and by replicating the design in the third dimension, complemented by temporal tuning of medium composition (when required) to address cellular maturation and different proliferation rates of multiple cell types.

4.3 Temperature control and power requirements

Temperature measurements confirmed that temporal variations in ambient temperature resulted in no more than ±0.2°C fluctuations about the controlled value. Temperature stability was partly ascribed to the small system volume (small inertia) and partly to the use of forced convection heat and mass transport.

In small-scale devices, the maintenance of a spatially uniform environmental parameter is often easier and cheaper to realize than in standard systems where large volumes contribute to gradients of a controlled parameter such as temperature or concentration. Miniaturization facilitates the control and often leads to faster response to physical and chemical changes with negligible delays in reaching steady operation (Voldman et al. 1999). As demonstrated with thermal control, steady temperature was achieved within 45 min and the delay in response to

changes in ambient temperature was negligible (±0.2°C). By contrast, in large-scale incubators the response time of the feedback control loop is typically longer and may cause significant oscillations of a regulated parameter.

Since the temperature of medium in the withdrawal chamber follows that of the injected medium, the spatial variability in sample temperature was not considered significant. This is important for homeostatic control as cellular metabolic demands and biophysical function depend on spatially uniform and temporally stable temperature. This may also enable the design reduction to a single sensor external to the culture (in the withdrawal chamber) to control the sample temperature.

Commercial technologies offer a number of approaches to regulate the sample temperature during imaging including microscope stage warmers, objective heating, heating of the bathing medium or the entire enclosure surrounding the microscope. The downsides of these strategies include the development of temperature gradients within the sample, high conductive thermal resistance, high power consumption, the shifting of imaging plane, unstable control, contamination or bulky infrastructure either alone or in combination. The design presented herein alleviates much of these problems by way of a sterile, imaging accessible membrane aerator; and small volume and low thermal time constants due to convective gas heating rather than conduction. Note that the provisions for high numerical aperture imaging using immersion objectives were incorporated but this capability was outside the scope of developments and validations presented herein.

In practice, the heater dissipated less than 3 Watts. Low power consumption and forced convection heat transport facilitate system design and allow battery operation. However, insulation, higher temperature variations within the enclosure (but not the sample) and short-loop gas recirculation each reduce this power demand. For example, clear insulating tapes may be placed on all exterior surfaces of the incubator except for the imaging surface. The additional thermal resistance of a tape and a high contact thermal resistance between the tape and the wall may be exploited to further reduce the heat loss or to improve the temperature uniformity.

4.4 Comparison with bioreactor-based technologies

3D culture systems are attractive candidates for *in vitro* experimentation and the production of cell culture derived drugs such as monoclonal antibodies, insulin, interferon and erythropoietin (Kostov et al. 2001; Wang et al. 2005). While the bioreactor technology has been modified for large sample volume screening applications, the limitations still include low-throughput, high operating costs, and the inability to continuously monitor cells long-term (Kostov et

al. 2001; Wang et al. 2005). We have designed the perfusion chamber and the incubator to enable imaging access in an adaptive and scalable format. A comparatively small volume of the culture chamber (under $10\,\mu L$) allows rapid exchange rates, facilitates control, and reduces reagent consumption.

Bioreactor technologies face significant challenges. First, to increase the production of pharmaceuticals or viral vectors for clinical gene therapy, high-density cultivation of animal cells ($>10,000$ cells/mm^3) is required (Wang et al. 2005). We have shown that we can sustain brain tissue mimetic primary cell co-cultures at 50,000 cells/mm^3. Second, to regenerate tissue and to reproduce viable cells that are difficult to culture in traditional culture systems, a 3D *in vivo* like extracellular environment is necessary. We have shown that we can culture at least 0.45 mm thick co-cultures using forced convection of the nutrient medium through the mass of cells at exchange rates that are orders of magnitude higher than those realized using passive diffusion and capillary action.

4.5 Intra-culture environment control

Many factors affect the culturing of animal cells at high densities including pH, temperature, dissolved O_2 concentration, nutrient consumption, serum, growth factors, ECM, fluctuations in culture condition, the accumulation of catabolites, normal and shear stresses among others.

While forced convection intra-culture perfusion may improve the viability of tissue mimetic cultures, the success of this perfusion method depends on the content and the concentration of relevant agents in the nutrient medium. Cell culture media are formulated for planar cultures lacking 3D cell-cell and cell-matrix soluble cues and are often suitable for monotypic rather than heterotypic cultures of cells. However, even for planar cultures the media composition may require optimization to address cellular maturation. When the circulation mimicking nutrient perfusion lacks the necessary constituents to support the culture, culture degenerates regardless of perfusion. The ECM affects solute transport through both diffusion and convection, the binding of compounds such as growth factors and cell-ECM signaling. Therefore the medium should be 3D culture specific and tailored to both the actual heterogeneous population of cells and the ECM to exploit the full potential of the intra-culture perfusion. In addition, the ECM and actively controlled intra-culture perfusion may be further implemented to mirror the physiological shear stresses and rhythmic interstitial flow pulsations in cardiac and other tissue equivalents known to respond to such mechanical stimuli.

The mass equilibrated withdrawal of depleted medium and catabolites from the culture chamber prevents the accumulation of otherwise toxic waste products within the

3D culture. The gas exchange through the culture top, via semi-permeable membrane, facilitates the maintenance of physiological pH and dissolved gas concentration. It is known, however, that a few hours viable acute cortical slices may not exceed ~500 μm in plating thickness due to low interstitial concentration of dissolved O_2 (Yamamoto and McIlwain 1966). Analogous limitation in 3D culture thickness may be alleviated using an optional, heated and vented aerator placed upstream of the perfusion chamber (Fig. 8) to equilibrate the injected medium. With this provision, the culture is provided with gas through both its top surface (gas-permeable membrane) and its bottom surface (via equilibrated medium), to augment the O_2 tension in the culture middle. Notably, this aerator also serves as a heated bubble trap and consists of a tee with a semi-permeable membrane stretched over its vertical leg and sealed by a vented end-cap.

Perfused 3D culture incubator was designed to provide stable culturing conditions to minimize the experimental uncertainty linking culture environment and cell behavior. In unperfused systems, whether 2D or 3D, periodic medium replacement causes the fluctuations in culture condition that may substantially alter cell physiology and function (Wu et al. 2007). The same is true for inadequately perfused cultures, where diffusive limitations cause temporal variations in culture condition due to unmet metabolic requirements. This may be mitigated by intra-culture convective perfusion at an adequate flow rate to realize relatively homogeneous and temporally invariant cellular microenvironment throughout the culture. Another common cause of fluctuations in culture condition is due to variability in culture temperature during culture removal from the incubator for routine inspections, feedings and other manipulations. These and other concerns including the inconsistency in intra-culture pH and gas concentration could be mitigated using disclosed design.

5 Conclusions

A growing area in the field of tissue engineering is the development of tissue equivalents as model systems for *in*
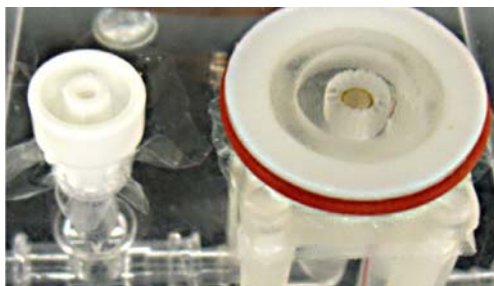
Fig. 8 The aerator of injected medium

vitro experimentation and high-throughput screening applications (Fox et al. 2006; Hicks et al. 2006; Mueller-Klieser 1997; Schindler et al. 2006). Unfortunately, thick, high-density tissue equivalents are difficult to maintain similar to the thick sections of explanted tissue they are approximating. By way of forced convection interstitial perfusion we have shown that we can reproducibly culture brain tissue mimetics at cell densities that are approaching those *in vivo*. Together, microfluidics and 3D cultures may become a powerful framework: *microfluidic engineered tissue mimetics* for disease studies and therapeutic interventions due to inherent advantages of an *in vitro* format enhanced by convective mass transport that not only supports the culture but becomes an intermediate pre-animal test-bed and the exclusive delivery vehicle for large molecule drugs (Swartz and Fleury 2007).

While cell culture is an essential tool for biotechnology and pre-clinical science, an accessible, laboratory-scale cell culture and analysis system has yet to be realized. Developed perfusion and incubation methodologies may be useful in this regard. Miniature incubator with integrated microfluidic perfusion chamber enables simultaneous 3D culturing, non-invasive monitoring and experiments on a bench top or a microscope stand. Fluidic, optical and electrical accessibility of the system simplify environmental control, culture manipulations and studies. Optical access allows imaging, including functional imaging *in vitro*, for which forced intra-culture perfusion may be an asset to administer agents or dyes and to prevent the assay variability due to culture decay. Modular design allows the integration and interfacing of various components to suit particular application challenges while maintaining stability and consistency of culture condition in laboratory or *in situ*. Reproducible extended culturing of thick 3D tissue-mimetic cultures will provide higher fidelity to *in vivo* function in a much needed dynamically controlled and accessible environment than currently attainable in cell-based assays and regenerative medicine.

Appendix

$$Q_1 = U \cdot A \cdot \Delta T \tag{1}$$

$$U = (t/k + 1/h)^{-1} \tag{2}$$

$$Q_2 = \rho \cdot \dot{V} \cdot (h_o - h_i) \tag{3}$$

$$\dot{V}_a = (Q_1 + Q_2)\big/\big[\rho_a \cdot c_p \cdot \big(T_{a,h} - T_{a,o}\big)\big] \qquad (4)$$

$$Q_h = \rho_a \cdot \dot{V}_a \cdot c_p \cdot \big(T_{a,i} - T_{a,h}\big) \qquad (5)$$

$$L = Q_2\big/\big(\overline{h} \cdot \pi \cdot D \cdot \Delta T_{lm}\big) \qquad (6)$$

$$\Delta T_{lm} = (\Delta T_o - \Delta T_i)/\ln(\Delta T_o/\Delta T_i) \qquad (7)$$

$$\overline{h} = N_u \cdot k/D \qquad (8)$$

$$l = 0.05 \cdot R_{eD} \cdot P_r \cdot D \qquad (9)$$

References

N.H. Bass, H.H. Hess, A. Pope, C. Thalheimer, J. Comp. Neurol. **143**, 481 (1971). doi:10.1002/cne.901430405

S.N. Bhatia, U.J. Balis, M.L. Yarmush, M. Toner, FASEB J. **13**, 1883 (1999)

N.J. Boudreau, P.L. Jones, Biochem. J. **339**, 481 (1999). doi:10.1042/0264-6021:3390481

K. Brannvall, K. Bergman, U. Wallenquist, S. Svahn, T. Bowden, J. Hilborn, K. Forsberg-Nilsson, J. Neurosci. Res. **85**, 2138 (2007). doi:10.1002/jnr.21358

V. Braitenberg, J. Comput. Neurosci. **10**, 71 (2001). doi:10.1023/A:1008920127052

O. Caspi, A. Lesman, Y. Basevitch, A. Gepstein, G. Arbel, I.H. Habib, L. Gepstein, S. Levenberg, Circ. Ress. **100**, 263 (2007). doi:10.1161/01.RES.0000257776.05673.ff

C.S. Chen, M. Mrksich, S. Huang, G.M. Whitesides, D.E. Ingber, Science **276**, 1425 (1997). doi:10.1126/science.276.5317.1425

Y. Choi, J. Vukasinovic, A. Glezer, M.G. Allen, Biomed. Microdevices. **10**, 437 (2008). doi:10.1007/s10544-007-9153-4

D.K. Cullen, J. Vukasinovic, A. Glezer, M.C. Laplaca, J. Neural. Eng. **4**, 159 (2007). doi:10.1088/1741-2560/4/2/015

J.W. Deitmer, Respir. Physiol. **129**, 71 (2001). doi:10.1016/S0034-5687(01)00283-3

R.P. Dring, J. Fluid. Eng.-T ASME **104**, 15 (1982)

Editorial, Nature **424**, 861 (2003) doi: 10.1038/424861b

J. El-Ali, P.K. Sorger, K.F. Jensen, Nature **442**, 403 (2006). doi:10.1038/nature05063

M.V. Fournier, K.J. Martin, J. Cell Physiol. **209**, 625 (2006). doi:10.1002/jcp.20787

S. Fox, S. Farr-Jones, L. Sopchak, A. Boggs, H.W. Nicely, R. Khoury, M. Biros, J. Biomol. Screen. **11**, 864 (2006). doi:10.1177/1087057106292473

P.L. Gabbott, M.G. Stewart, Neuroscience **21**, 833 (1987)

K.O. Hicks, F.B. Pruijn, T.W. Secomb, M.P. Hay, R. Hsu, J.M. Brown, W.A. Denny, M.W. Dewhirst, W.R. Wilson, J. Natl. Cancer. Inst. **98**, 1118 (2006). doi:10.1093/jnci/djj306

F.P. Incropera, D.P. DeWitt, *Fundamentals of heat and mass transfer*, 5th edn. (J. Wiley, New York, 2002)

P.A. Kenny, M.J. Bissell, Int. J. Cancer **107**, 688 (2003). doi:10.1002/ijc.11491

C.J. Kirkpatrick, R.E. Unger, V. Krump-Konvalinkova, K. Peters, H. Schmidt, G. Kamp, J. Mater. Sci. Mater. Med. **14**, 677 (2003)

Y. Kostov, P. Harms, L. Randers-Eichhorn, G. Rao, Biotechnol. Bioeng. **72**, 346 (2001). doi:10.1002/1097-0290(20010205)72:3<346::AID-BIT12>3.0.CO;2-X

S.A. Lelievre, V.M. Weaver, J.A. Nickerson, C.A. Larabell, A. Bhaumik, O.W. Petersen, M.J. Bissell, Proc. Natl. Acad. Sci. USA **95**, 14711 (1998). doi:10.1073/pnas.95.25.14711

S. Levenberg, J. Rouwkema, M. Macdonald, E.S. Garfein, D.S. Kohane, D.C. Darland, R. Marini, C.A. van Blitterswijk, R.C. Mulligan, P.A. D'Amore, R. Langer, Nat. Biotechnol. **23**, 879 (2005). doi:10.1038/nbt1109

H. Liu, S.F. Collins, L.J. Suggs, Biomaterials **27**, 6004 (2006). doi:10.1016/j.biomaterials.2006.06.016

P.J. Magistretti, J. Exp. Biol. **209**, 2304 (2006). doi:10.1242/jeb.02208

W. Mueller-Klieser, Am. J. Physiol. **273**, C1109 (1997)

S.M. Potter, T.B. DeMarse, J. Neurosci. Methods **110**, 17 (2001). doi:10.1016/S0165-0270(01)00412-5

J. Rouwkema, N.C. Rivron, C.A. van Blitterswijk, Trends Biotechnol. **26**, 434 (2008). doi:10.1016/j.tibtech.2008.04.009

J.G. Santiago, S.T. Wereley, C.D. Meinhart, D.J. Beebe, R.J. Adrian, Exp. Fluids **25**, 316 (1998). doi:10.1007/s003480050235

M. Schindler, E.K.A. Nur, I. Ahmed, J. Kamal, H.Y. Liu, N. Amor, A. S. Ponery, D.P. Crockett, T.H. Grafe, H.Y. Chung, T. Weik, E. Jones, S. Meiners, Cell Biochem. Biophys. **45**, 215 (2006). doi:10.1385/CBB:45:2:215

K.S. Smalley, M. Lioni, M. Herlyn, In Vitro Cell Dev. Biol. Anim. **42**, 242 (2006). doi:10.1290/0604027.1

L. Stoppini, P.A. Buchs, D. Muller, J. Neurosci. Methods **37**, 173 (1991)

F. Sultan, V. Braitenberg, J. Hirnforsch. **34**, 79 (1993)

M.A. Swartz, M.E. Fleury, Annu. Rev. Biomed. Eng. **9**, 229 (2007). doi:10.1146/annurev.bioeng.9.060906.151850

C.H. Thomas, J.H. Collier, C.S. Sfeir, K.E. Healy, Proc. Natl. Acad. Sci. USA **99**, 1972 (2002). doi:10.1073/pnas.032668799

M. Tsacopoulos, P.J. Magistretti, J. Neurosci. **16**, 877 (1996)

J. Voldman, M.L. Gray, M.A. Schmidt, Annu. Rev. Biomed. Eng. **1**, 401 (1999). doi:10.1146/annurev.bioeng.1.1.401

D. Walpita, E. Hay, Nat. Rev. Mol. Cell. Biol. **3**(2), 137 (2002). doi:10.1038/nrm727

D. Wang, W. Liu, B. Han, R. Xu, Curr. Pharm. Biotechnol. **6**, 397 (2005)

V.M. Weaver, O.W. Petersen, F. Wang, C.A. Larabell, P. Briand, C. Damsky, M.J. Bissell, J. Cell Biol. **137**, 231 (1997)

R.W. Williams, K. Herrup, Annu. Rev. Neurosci. **11**, 423 (1988). doi:10.1146/annurev.ne.11.030188.002231

M.H. Wu, J.P. Urban, Z.F. Cui, Z. Cui, X. Xu, Biotechnol. Prog. **23**, 430 (2007). doi:10.1021/bp060024v

C. Yamamoto, H. McIlwain, J. Neurochem. **13**, 1333 (1966). doi:10.1111/j.1471-4159.1966.tb04296.x

M.H. Zaman, L.M. Trapani, A.L. Sieminski, D. Mackellar, H. Gong, R.D. Kamm, A. Wells, D.A. Lauffenburger, P. Matsudaira, Proc. Natl. Acad. Sci. U.S.A. **103**, 10889 (2006). doi:10.1073/pnas.0604460103